tvst

https://doi.org/10.1167/tvst.7.6.20

Article

Enhanced Quantification of Retinal Perfusion by Improved Discrimination of Blood Flow From Bulk Motion Signal in OCTA

Acner Camino[1], Miao Zhang[2], Liang Liu[1], Jie Wang[1], Yali Jia[1], and David Huang[1]

[1] Casey Eye Institute, Oregon Health & Science University, Portland, OR, USA
[2] Optovue, Inc., Fremont, CA, USA

Correspondence: David Huang, Casey Eye Institute, Oregon Health & Science University, Portland, OR 97239, USA. e-mail: huangd@ohsu.edu

Received: 12 July 2018
Accepted: 10 October 2018
Published: 6 December 2018

Keywords: OCTA; vessel density; motion artifacts

Citation: Camino A, Zhang M, Liu L, Wang J, Jia Y, Huang D. Enhanced quantification of retinal perfusion by improved discrimination of blood flow from bulk motion signal in OCTA. Trans Vis Sci Tech. 2018;7(6): 20, https://doi.org/10.1167/tvst.7.6.20

Purpose: Quantification of optical coherence tomography angiography (OCTA) is confounded by the prevalence of bulk motion. We have previously developed a regression-based bulk motion subtraction (rb-BMS) algorithm that estimates bulk motion velocity and corrects for its effect on flow signal. Here, we aim to investigate its ability to improve the reliability of capillary density (CD) quantification.

Methods: Two spectral-domain systems (70-kHz Avanti/AngioVue and 68-kHz Cirrus/AngioPlex) acquired 6 × 6-mm OCTA scans. The rb-BMS algorithm was applied on each OCTA volume. Regression analysis of angiographic versus reflectance signal of avascular A-lines in B-frames was used to set an optimized reflectance-adjusted threshold for discriminating vascular versus nonvascular voxels. The CD was calculated from en face maximum projections of the superficial vascular complex in macular scans and the nerve fiber layer plexus in disc scans, excluding large vessels. The retinal signal strength (RSS) was calculated by averaging the logarithmic-scale OCT reflectance signal, and its correlation with CD was investigated.

Results: Eight healthy eyes were scanned with each instrument on 2 separate days. The rb-BMS algorithm improved within-visit repeatability and between-visit reproducibility of CD compared with a global-threshold measurement algorithm. Using the rb-BMS algorithm, the CD results were less affected by RSS and the population variation was reduced. Motion-induced line artifacts were also reduced.

Conclusions: The rb-BMS algorithm improved the reliability of perfusion quantification in OCTA on both Food and Drug Administration–cleared spectral-domain OCTA systems.

Translational Relevance: The rb-BMS method helped reduce the inter-scan variability by generating accurate vessel maps, improving the reliability of retinal perfusion quantification.

Introduction

Optical coherence tomography angiography (OCTA)[1–4] is a useful clinical tool for the early diagnosis and progress evaluation of diseases that affect ocular circulation. Based on the variation of OCT signal between scans at the same location, OCTA algorithms can provide depth-resolved information about microvascular anomalies without exogenous contrast agents. To date, commercial OCTA systems have been successful in visualizing retinal flow (or lack thereof) but have found challenging to deliver reliable quantification of the microvascular density, owing to the prevalence of artifacts and the strong dependence on reflectance signal strength.

Motion artifacts appear in OCTA images because of eye motion in the time it takes the OCT system to complete two consecutive B-scans. Consequently, nonvascular tissues can acquire flow signal, making them difficult to differentiate from blood vessels. The flow signal in vascular tissue can be boosted, making measurement of velocity or flow index inaccurate. In the event of rapid microsaccadic motion (rapid

repositioning during fixation), the bulk tissue motion overwhelms capillary flow signal and the entire OCTA B-frame (bright white line artifact on en face OCTA) must be discarded and replaced using real-time tracking or postprocessing registration with a redundant volume. But in most of the OCTA volume there is contribution to flow signal from slower bulk motion due to drift, pulsation, or tremors. These need to be subtracted so that the clean signal from blood flow can be retrieved.

We have recently proposed a fully automated method that separates vascular from nonvascular voxels, and removes the contribution of bulk motion from flow signal in vascular voxels.[5] Our novel algorithm is based on two insights. One is that the decorrelation signal due to bulk motion is dependent on both bulk motion velocity and reflectance signal amplitude, therefore, the velocity could be recovered by regression analysis. Two is that because velocity and decorrelation signals are nonlinearly related, subtraction of bulk motion should be done after the nonlinear conversion of decorrelation to velocity. In the first report of this regression-based bulk-motion subtraction (rb-BMS) algorithm,[5] we demonstrated improved visualization and reduced vessel density variability compared with another algorithm that simply subtracted the median decorrelation value (a simplistic estimate of bulk motion signal) within retinal slab. In this paper, we investigate whether the rb-BMS algorithm can improve the reliability of perfusion quantification in commercial OCTA systems by reducing the interscan variability of capillary density as well as its dependence on retinal signal strength (RSS). Additionally, we compare the prevalence of bulk motion artifacts before and after applying the regression-based subtraction scheme. Finally, we investigate the efficiency of the algorithm in suppressing bulk motion noise on OCTA of healthy and diabetic retinopathy subjects as well as preserving vascular integrity.

Methods

Study Population

Healthy volunteers were recruited at the Casey Eye Institute at the Oregon Health & Science University (OHSU). The protocol was approved by the institutional review board/Ethics Committee of OHSU and the research adhered to the tenants of the Declaration of Helsinki.

Data Acquisition

Participants were imaged with the following two commercial spectral-domain OCT/OCTA systems: the Avanti-AngioVue (Optovue, Inc. Fremont, CA) and the Cirrus-AngioPlex (Zeiss Medical Technology, Dublin, CA). Both systems operate at a central wavelength of 840 nm, respective bandwidths of 45 and 50 nm and respective A-scan rates of 70 and 68 kHz.

Scans covered an area of 6×6 mm^2 and were either centered at the fovea or the optic disc. For the AngioVue, each dataset consisted of two scans acquired at orthogonal scanning directions (horizontal priority and vertical priority). A volume consisted of two repeated B-scans at 400 locations (800 B-scans total) with each B-scan consisting of 400 A-scans. Acquisition of frames affected by microsaccadic artifacts and blinking were minimized by real-time eye tracking based on an infrared (IR) fundus camera.[6] Structural and angiography data were acquired simultaneously on each volumetric scan. Blood flow was detected with the split-spectrum amplitude decorrelation angiography (SSADA) algorithm, which computes the decorrelation between consecutive B-scans at the same position.[7] OCT structural images were generated by averaging the two repeated B-scans. In addition, the two scans were registered and merged into a third volume by Optovue's Motion Correction Technology (MCT)[8] and processed by the Angioanalytics software (Optovue, Inc.).

For the AngioPlex, the volumetric scan has horizontal priority. Its FastTrac real-time tracking technology reduced microsaccadic artifacts. Four repeated B-scans were acquired at each of 350 lateral positions. Each B-scan comprised 350 A-lines. The optical microangiography (OMAG) algorithm generated flow signal by comparing the repeated B-scans.[9]

Data Processing

A directional graph search method developed by Zhang et al.[10] was used to segment the retinal layers comprising the superficial vascular complex (SVC), the inner retina as well as the Bruch's membrane. The SVC slab was defined as the superficial 80% of the ganglion cell complex (GCC),[11] the inner retinal slab was defined between the inner limiting membrane (ILM) and the outer boundary of the outer plexiform layer (OPL) and the retinal slab was defined between ILM and the Bruch's membrane.

Our rb-BMS software was applied directly to

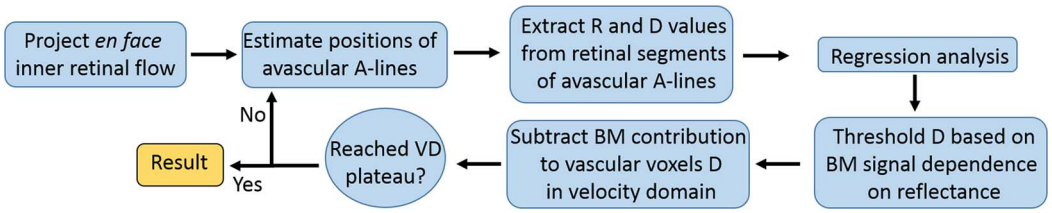

Figure 1. Flowchart of the regression-based bulk motion subtraction algorithm. R, reflectance; D, decorrelation; BM, bulk motion; VD, vessel density.

AngioPlex scans because there is no registration of multiple scans involved. For Avanti/AngioVue scans it was applied separately to the horizontal and vertical priority scans upstream of the MCT volume merge. Briefly, the rb-BMS algorithm estimates the bulk motion velocity by linear regression analysis of decorrelation versus reflectance in preliminarily identified nonvascular voxels in each B-frame (Fig. 1).[5] The regression analysis yields a reflectance-adjusted range for bulk-motion–related decorrelation value; voxels within this range are identified as nonvascular and their flow signal values were set to zero. Voxels with decorrelation values above the bulk-motion threshold were identified as vascular voxels. For vascular voxels, the bulk motion velocity is subtracted using a nonlinear model that relates decorrelation (flow) signal to erythrocyte velocity. The model was calibrated using a laboratory phantom that used ex vivo human blood flowing through a microfluidic chip.[12,13]

In order to perform regression analysis of bulk motion, we first identified the A-lines devoid of blood flow. In our previous report, we chose A-lines with the lowest 10 percentile of maximum projected flow signal. In this paper, we used a refined version of the rb-BMS algorithm that iteratively identified the nonvascular A-lines. The first iteration is the same as the previous version. But in subsequent iterations, the nonvascular A-lines were identified as those without any vascular voxels within the inner retina in the previous iteration. The iterations yield gradually increasing thresholds for vascular voxel identification and lower inner-retinal capillary density that eventually converges to a stable value (Fig. 2). This iterative refinement optimizes the data available for regression analysis and does not assume that all B-frames have similar number of nonvascular A-lines. Because we observed near convergence by the third iteration, for the remainder of the paper only three iterations are used for the rb-BMS algorithm. Data were processed using Matlab 2017a release (Mathworks, Natick, MA).

Capillary Density Quantification

We calculated the capillary density as the percentage of vascular voxels on en face projection angiograms, excluding large vessels. The positions of large vessels were detected using their large decorrelation values in the OCTA data and the shadows projected onto the outer retina in the reflectance OCT data.[5] The 0.6-mm diameter central circle was excluded on macular scans to reduce variation due to the size of the foveal avascular zone (FAZ). A 2-mm diameter circle centered (manually centered) on the disc was excluded on disc scans for the evaluation of peripapillary retinal capillary density.

Capillary density was calculated from binarized maps of en face OCTA of the nerve fiber layer plexus in disc scans and the SVC in macular scans. The rb-BMS algorithm achieves binary classification of vascular versus nonvascular voxels using the reflectance-adjusted threshold in each B-frame. For comparison, binarization was also generated by a global thresholding method. On AngioVue scans, the global threshold was applied on both the original horizontal and vertical priority scans before any bulk motion processing and also after AngioVue's proprietary processing. The thresholds selected were such that the mean capillary density of the population was the same from all quantification methods ($P > 0.05$). The capillary density repeatability was evaluated on healthy subjects by the pooled standard deviation of two scans in the same visit for AngioPlex and between a horizontal and a consecutive vertical priority acquisition for AngioVue. The reproducibility was evaluated by the pooled standard deviation between scans corresponding to visits separated by 1 week. To calculate the variability of the capillary density among all subjects, the capillary density of scans corresponding to the same subject were averaged and the standard deviation of the population was found. Finally, the capillary density dependence on scan quality was evaluated by assessing its correlation to a RSS, defined as the mean OCT reflectance value within the retinal slab.

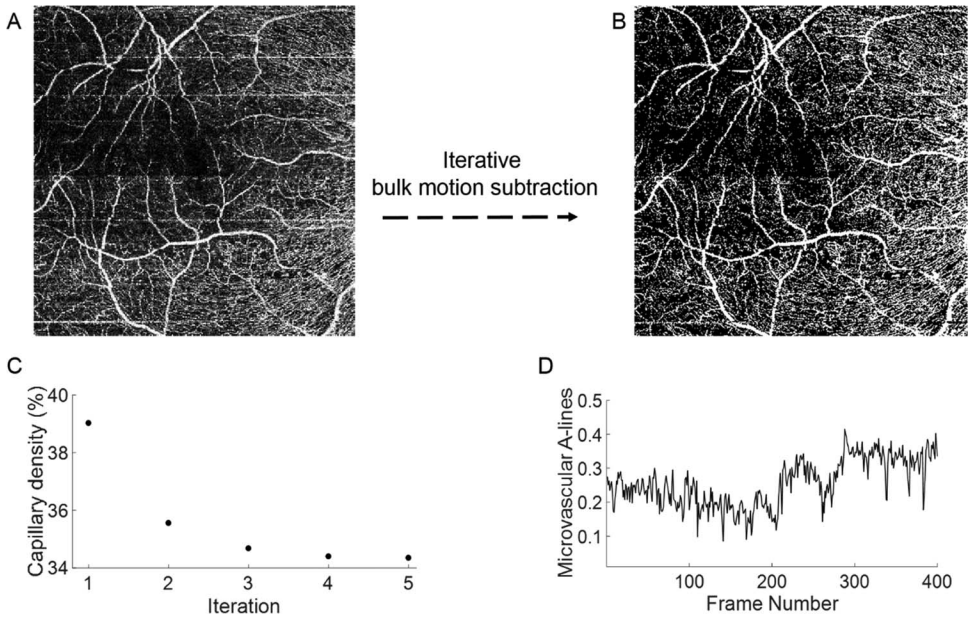

Figure 2. Breakdown of the rationale behind the selection of the avascular A-lines providing the reflectance and decorrelation data of background voxels for regression analysis. A horizontal priority scan acquired by Avanti/AngioVue corresponding to a diabetic retinopathy patient is shown. (A) Before processing, the en face angiogram of the inner retinal slab is generated by maximum projection of decorrelation values. Initially, the proportion of A-lines that do not contain vascular voxels is unknown. The proportion of microvascular A-lines (excluding large vessels) is initialized for all frames at 0.9 and the A-lines within the lowest 10 percentile of decorrelation values of the frame are selected to deliver the voxels used for regression analysis. After the bulk motion subtraction algorithm is run once, the microvascular A-lines are updated and the software runs again. Subtraction of the bulk motion artifacts is successful (B) without removing true capillaries because the capillary density (found as the percentage of microvascular pixels) converges to a certain value (C). Three iterations were sufficient for a successful implementation. The proportion of microvascular A-lines per frame at the last iteration (D) was in good agreement with qualitative observations in (B).

Image Quality Assessment

Vessel continuity was calculated to assess the extent to which the rb-BMS algorithms disrupted the connectivity of capillary pixels by misclassifying vascular pixels as nonvascular. We generated skeletonized versions of en face angiograms and calculated the percentage of voxels contained in connected groups with more than five voxels.

We also defined a motion prevalence metric to compare the predominance of artifacts before and after processing. Voxels at the coordinates of large vessels were first set to zero. Then, a high-pass filter was applied along the slow scanning axis. The inner-retinal vascular map was filtered (F) and averaged along the fast scanning axis as in Equation 1:

$$\mathrm{BM}_{Frame} = \frac{1}{width}\sum_{\substack{fast\\axis}} F \qquad (1)$$

where *width* is 350 for AngioPlex and 400 for AngioVue. Those frames for which the quantity BM_{Frame} in Equation 1 was larger than two standard deviations above the volume's mean value were considered artefactual and their percentage was a measure of motion prevalence.

The paired t-test was used to compare the means of parameters.

Results

Eight healthy subjects (29 ± 4-years old) were imaged by both commercial systems. At least two images of the macula and optic disc were acquired on the first visit and one image on the second visit for each system. No images were discarded. We first compared the qualitative improvement of the bulk motion subtraction by rb-BMS compared with the median subtraction algorithm in Zeiss AngioPlex and AngioVue. The rb-BMS method was better at removing the spurious signal caused by bulk motion, whereas preserving capillary signal in the binary masks of macular (Fig. 3) and optic disc scans (Fig. 4) for both OCTA instruments. In addition, the correlation between capillary density and RSS was

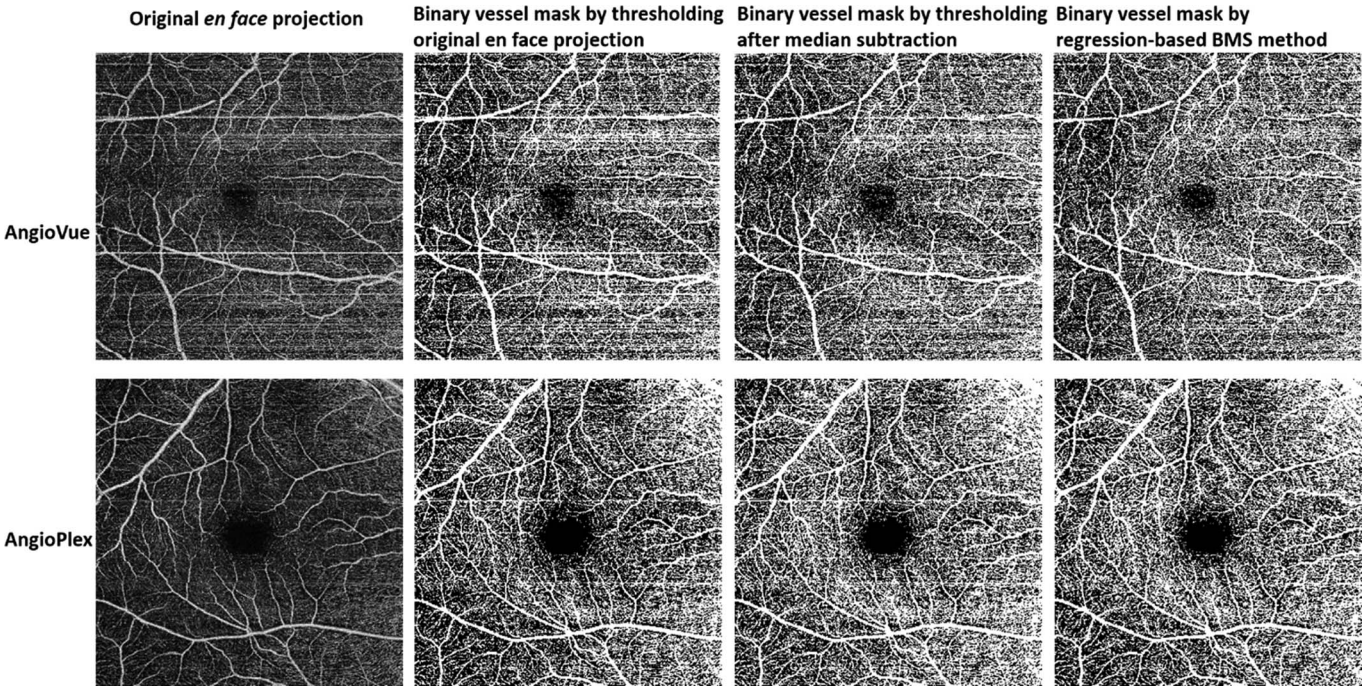

Figure 3. Comparison of vascular maps of the superficial vascular complex en face projection of a representative horizontal priority scan of a healthy subject generated by thresholding the original scan without bulk motion subtraction (BMS), median subtraction and the regression-based BMS algorithm. Scans acquired by both commercial systems used in this study are represented. Segmentation of the image corresponding to Optovue's BMS method is different because it was done on a different file, generated by RTVue software.

reduced for both macular and disc scans on both OCTA systems (Figs. 5, 6), indicating a reduced dependency of vascular thresholding on reflectance when the rb-BMS method is applied.

The repeatability and reproducibility of the capillary density of macular scans was improved by rb-BMS in the AngioVue instrument with respect to global thresholding and median subtraction (Tables 1, 2). For AngioPlex images the intervisit reproducibility of macular CD was also improved ($P < 0.05$) but the improvement in intravisit repeatability was not statistically significant (Tables 2, 3). The improvement in repeatability and reproducibility of retinal never fiber layer CD of disc scans was not statistically significant in either instrument ($P > 0.1$) (Table 2).

The motion prevalence metric was consistently lower after rb-BMS with respect to global thresholding on original and median subtraction images for macular and optic disc in both instruments (Tables 1–3). The lowest CD variability corresponded to the rb-

Table 1. Comparison of Quantitative Metrics Evaluating the Reliability of Three Methods Generating Macular Superficial Vascular Complex Maps

	Motion Prevalence	Vessel Connectivity	CD Repeatability	CD Reproducibility	Standard Deviation of Population
AngioPlex					
Global Th	1.1%	70.1%	1.8%	3.1%	3.9%
MS	0.6%	62.6%	2.0%	2.9%	3.5%
rb-BMS	0.4%	70.5%	1.1%	1.9%	3.9%
AngioVue					
Global Th	1.6%	64.7%	3.2%	2.3%	4.6%
MS	1.6%	68.2%	3.1%	2.6%	4.9%
rb-BMS	0.8%	65.0%	1.3%	1.2%	1.8%

Th, global thresholding; MS, global thresholding after median subtraction.

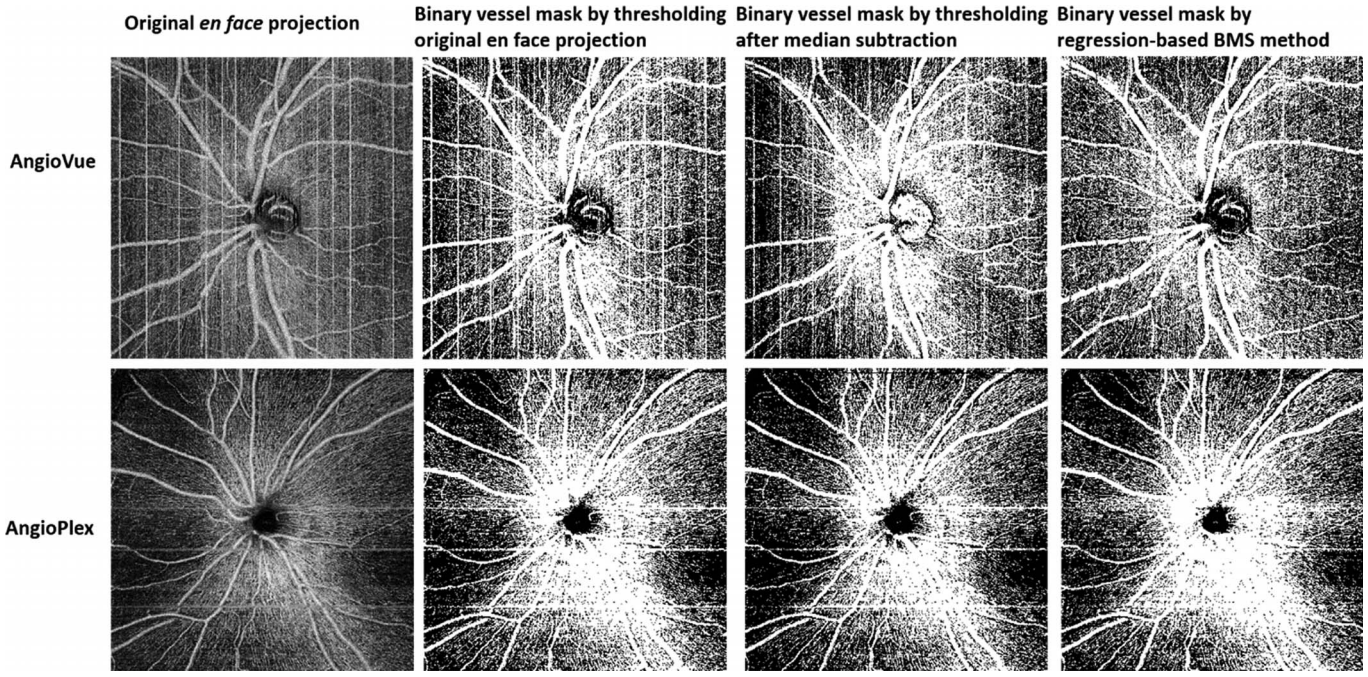

Figure 4. Comparison of vascular maps of the nerve fiber layer plexus en face projection of a representative scan of a healthy subject generated by thresholding the original scan without BMS, median subtraction, and the regression-based BMS algorithm. Scans acquired by both commercial systems used in this study are represented. Segmentation of the image corresponding to Optovue's BMS method is different because it was done on a different file, generated by RTVue software.

BMS method in all cases except macular images acquired by AngioPlex. The difference in vascular connectivity after the subtraction of bulk motion was not statistically significant ($P > 0.05$), indicating that the vascular network integrity was not particularly affected by rb-BMS.

The output of the AngioVue instrument is neither the horizontal or vertical priority scan, but an image that has undergone proprietary bulk-motion subtraction and further orthogonal registration and merging by MCT. Therefore, it is interesting to also compare the CD reproducibility and dependency on signal quality of the images processed by rb-BMS after MCT, with the values reported by Optovue's AngioAnalytics software (not available for 6 × 6-mm HD disc scans). Here, the dependency on signal

Table 2. Statistical Significance (*P* Values) of the Performance Improvement Achieved by the Rb-BMS Performance Over Global Thresholding of the Original and MS OCTA

	AngioPlex Macula	AngioPlex Disc	AngioVue Macula	AngioVue Disc
CD repeatability (standard deviation)				
MS < original	0.59	0.82	0.29	0.24
rb-BMS < original	0.28	0.2	<0.01	0.17
rb-BMS < MS	0.20	0.70	<0.05	0.75
CD reproducibility (standard deviation)				
MS < original	0.88	0.96	0.93	0.41
rb-BMS < Original	<0.05	0.22	<0.05	0.34
rb-BMS < MS	<0.05	0.19	<0.05	0.62
Prevalence of motion artifacts				
MS < original	<0.01	<0.05	>0.05	<0.01
rb-BMS < original	<0.01	<0.01	<0.01	<0.01
rb-BMS < MS	<0.05	<0.01	<0.01	<0.05

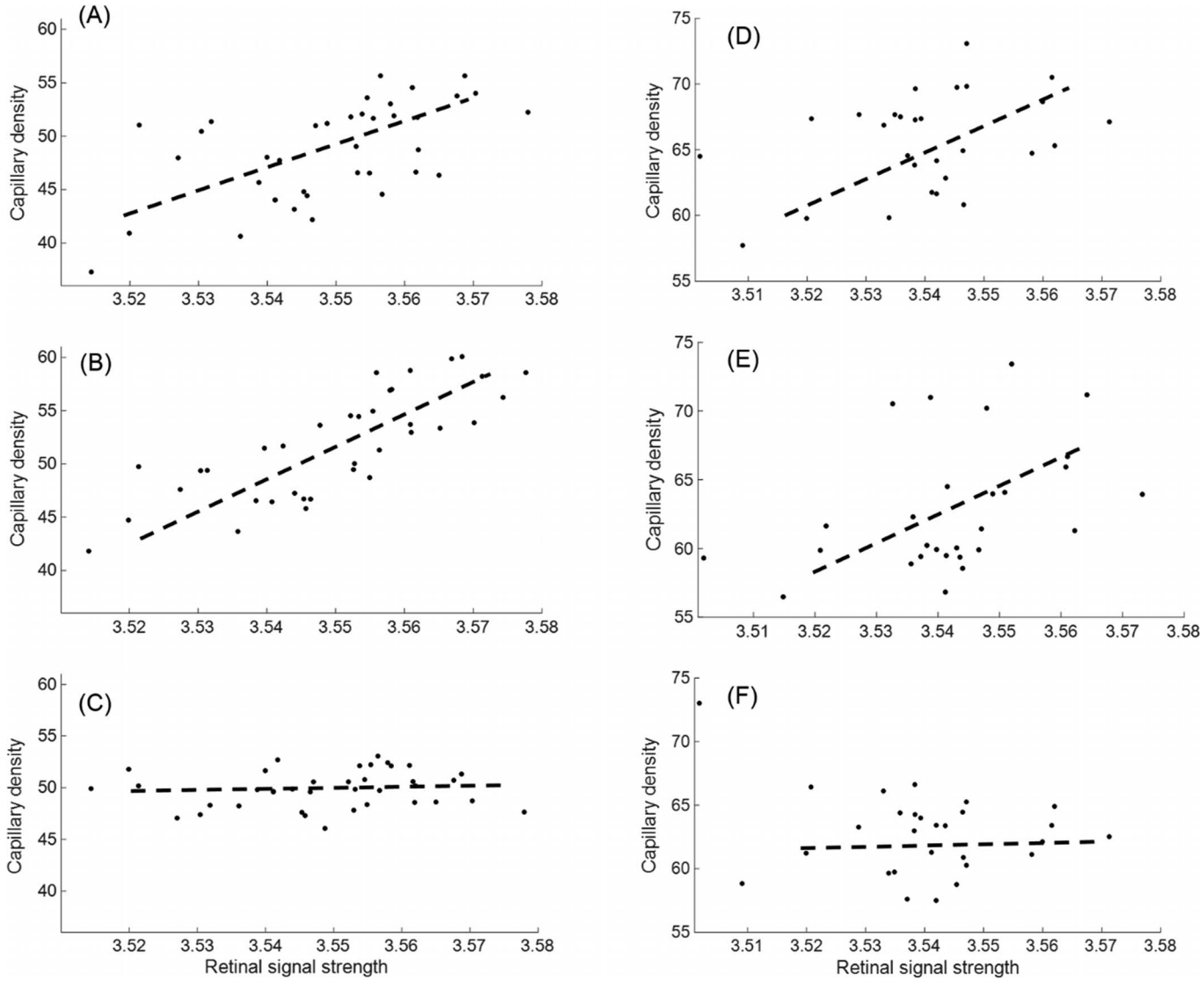

Figure 5. Correlation between CD and retinal signal strength is reduced by the rb-BMS algorithm on 28 macular (A–C) and disc (D–F) scans of healthy subjects acquired by the Avanti/AngioVue instrument. In macular scans, correlation between CD and signal strength changed from $R = 0.58$, $P < 0.01$ in the original image without BMS (A), to $R = 0.79$, $P < 0.01$ in the image processed by AngioVue's BMS (B), to $R = 0.12$, $P = 0.47$ in the image processed by rb-BMS (C). FAZ and large vessels are excluded. On disc scans, the correlation changed from $R = 0.39$, $P = 0.04$ in the original image without BMS (D), to $R = 0.42$, $P = 0.03$ in the image processed by AngioVue's BMS method (E), to $R = -0.24$, $P = 0.22$ in the image processed rb-BMS (F). Analytic zone is 4×4 mm, excluding the large vessels and a circle of 2-mm diameter centered at the disc.

quality was reduced for the rb-BMS data ($R = 0.12$, $P = 0.47$ for rb-BMS versus $R = 0.86$, $P < 0.01$ for AngioAnalytics), considering AngioAnalytics' signal strength index (SSI) native to this software as a measure of scan quality. The reproducibility of the horizontal/vertical priority scans processed by rb-BMS was not significantly improved (standard deviation 2.6% for AngioAnalytics versus 1.1% for rb-BMS, $P = 0.1$). However, CD quantification of scans merged by MCT after rb-BMS software had to be performed applying a global threshold, because images produced by our software could not be processed in AngioAnalytics.

Discussion

By applying the rb-BMS algorithm we have successfully reduced the prevalence of motion artifacts and, in consequence, the variability of CD quantification. In addition, we reduced the depen-

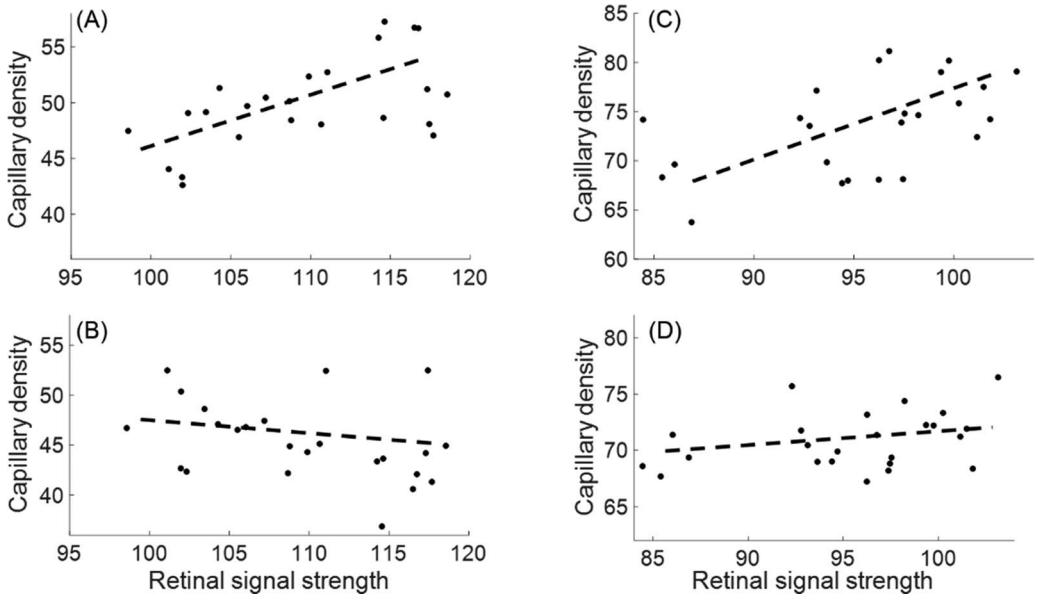

Figure 6. Correlation between CD and retinal signal strength is reduced by the rb-BMS algorithm on 24 macular (A, B) and disc (C, D) scans of healthy subjects acquired by the Cirrus/AngioPlex instrument. In macular scans, correlation between CD and signal strength changed from $R = 0.58$, $P < 0.01$ in the original image without BMS (A), to $R = -0.36$, $P = 0.08$ in the image processed by rb-BMS (B). FAZ and large vessels are excluded. On disc scans, the correlation changed from $R = 0.52$, $P = 0.01$ in the original image without BMS (C) to $R = 0.36$, $P = 0.09$ in the image processed by rb-BMS (F). Analytic zone is 4×4 mm, excluding the large vessels and a circle of 2-mm diameter centered at the disc.

dence of CD quantification on signal strength for disc and macular scans as well as improved the intervisit reproducibility on macular scans. The interscan variability of previous perfusion quantification methods is caused by a strong dependence of thresholding methods on the OCT reflectance of pixels and the prevalence of motion artifacts. Because background flow signal is larger in higher-reflectance pixels, global thresholding schemes usually misclassify background pixels to the vascular map, overestimating the actual CD. Also, because motion artifacts are unpredictable and cause the pixels in entire B-scans to be misclassified to the vascular map, they cause larger variability in the CD calculated from scans of the same eye. The rb-BMS method alleviates both disadvantages of the global thresholding scheme.

Commercial systems already implement hardware and software techniques to reduce these bulk motion artifacts. The recording of microsaccades and blinks can be prevented by tracking-assisted scanning[6] and the disjunction between consecutive frames during microsaccades can be corrected by volumetric registration of multiple scans.[8] However, tracking systems must be compromised in the severity of artifacts

Table 3. Comparison of Quantitative Metrics Evaluating the Reliability of Three Methods Generating Peripapillary Nerve Fiber Layer Plexus Vascular Maps

	Motion Prevalence	Vessel Connectivity	CD Repeatability	CD Reproducibility	Standard Deviation of Population
AngioPlex					
Global Th	1.4%	71.7%	2.0%	3.1%	4.9%
MS	0.6%	66.9%	2.0%	2.9%	3.0%
rb-BMS	0.3%	67.0%	1.2%	1.9%	2.5%
AngioVue					
Global Th	1.4%	66.9%	2.7%	3.1%	3.7%
MS	1.0%	73.7%	2.4%	2.3%	4.7%
rb-BMS	0.8%	69.0%	2.2%	1.9%	3.1%

detected, allowing small bulk motion to be recorded in order to complete scans successfully within a reasonable time. Moreover, tracking is difficult in regions absent of distinguishable features, such as in the peripheral retina, which have gained popularity for ultrawide-field OCTA imaging.[14–16] In consequence, small bulk motion is unavoidable in OCTA acquisition and must be reduced by postprocessing.

The traditional way to further reduce the bulk-motion contribution to flow signal by software is to subtract the median value of flow signal within retinal tissue in each B-frame.[17] However, a limitation of the median subtraction algorithm is that it does not solve the question of what threshold should we apply to generate a vascular map. Previously, the generation of the vascular maps used for quantification of perfusion has largely relied on global thresholding schemes. This approach is inadequate for microvascular quantification because it is highly dependent on the scan quality. Adaptive local thresholding based on regional signal-to-noise ratio (SNR) has been used as alternative to homogenize the vascular map in regions with low SNR.[18] However, the thresholds imposed are subjective and might artificially misclassify noise pixels into the vascular map.

We had previously reported a method that could already compensate the dependence of perfusion quantification on tissue reflectance and generate more accurate vascular maps of the en face image.[19] The approach we report here is superior to the previous alternatives in the following two aspects: it generates reflectance-adjusted vascular maps in three dimensions and reduces significantly the contribution of motion artifacts to microvascular density. Because this algorithm is applied on the whole OCTA volume, using it together with projection-resolved OCTA could be helpful in diseases that affect the perfusion of the deep capillary plexus, such as diabetic retinopathy and inherited retinal degeneration.

Besides thresholding, other methods for the generation of vascular maps and quantification of the vessel density have been proposed in the literature, such as application of vascular filters[20–22] and fractal analysis.[23,24] Although these solutions were developed expressly to relieve the issues with global thresholding schemes, careful inspection of their binarized maps shows that they are also prone to signal loss in regions with lower SNR,[21] they alter the microvascular caliber[20] and could even artificially connect flow voids between distinct vasculature. It is also worth noting that these filters are increasingly difficult to implement with accuracy in larger field-of-view images due to the reduced sampling density. Conversely, the vascular maps obtained by the rb-BMS algorithm not only provided repeatable capillary density, but also resembled the expected qualitative appearance of the capillary network.

The perfusion metric reported in this study was the capillary density rather than vessel density, for which we have excluded large arteries and veins in both disc and macular scans by a method reported previously in reference.[5] The capillary density is a measure of microvascular perfusion and should be more sensitive to small microvascular changes in the early stages of retinal diseases. As faster OCTA systems begin to allow imaging of larger regions of interest,[25] excluding the contribution of large vessel pixels from the quantification of vascular density seems more suitable to detect early microvascular dropout[26,27] in the peripheral retina.

A potential clinical application for improving quantification of OCTA metrics by the rb-BMS method is the cleanup of ischemic areas in diabetic retinopathy.[28] Algorithms that quantify the extent of microvascular damage rely on the generation of binarized vascular maps[29] and suffer from the same disadvantages of conventional thresholding schemes discussed above. Application of the rb- BMS algorithm in a diabetic retinopathy case showed good cleanup of capillary dropout areas (Figs. 1A, 1B) and hence, impaired capillary perfusion was better appreciated.

In summary, OCTA postprocessed by the rb-BMS algorithm can remove motion artifacts better than the median subtraction algorithm in currently Food and Drug Administration–approved commercial OCTA systems, AngioVue and AngioPlex, which used two different OCTA algorithms. Consequently, variability in the quantification of vascular density caused by random prevalence of motion in the healthy population was reduced. Moreover, the dependency of quantification on signal strength was significantly reduced by rb-BMS. Finally, because this is a voxel-wise, three-dimensional scheme, it has potential to be applied in tandem with projection-resolved OCTA for quantification of the in situ vascular density of the intermediate and deep capillary plexuses as well as the choriocapillaris.

Acknowledgments

Supported by Grants R01EY027833, DP3 DK104397, R01 EY024544, R01 EY023285, P30

EY010572, T32 EY023211-05 from the National Institutes of Health (Bethesda, MD), and an unrestricted departmental funding grant and William & Mary Greve Special Scholar Award from Research to Prevent Blindness (New York, NY), and the Antonio Champalimaud Vision Award.

Disclosure: **A. Camino**, Optovue, Inc. (P); **M. Zhang**, employed by Optovue, Inc. during the preparation of this manuscript (E); **L. Liu**, None; **J. Wang**, None; **Y. Jia**, has a significant financial interest in Optovue, Inc. (F, P); **D. Huang**, has a significant financial interest in Optovue, Inc. (F, I, P, R)

References

1. Jia Y, Tan O, Tokayer J, et al. Split-spectrum amplitude-decorrelation angiography with optical coherence tomography. *Opt Express*. 2012;20:4710–4725.
2. Gao SS, Jia Y, Zhang M, et al. Optical coherence tomography angiography. *Invest Ophthalmol Vis Sci*. 2016;57:OCT27–OCT36.
3. Kashani AH, Chen C-L, Gahm JK, et al. Optical coherence tomography angiography: a comprehensive review of current methods and clinical applications. *Prog Retin Eye Res*. 2017;60:66–100.
4. Chen C-L, Wang RK. Optical coherence tomography based angiography [Invited]. *Biomed Opt Express*. 2017;8:1056–1082.
5. Camino A, Jia Y, Liu G, Wang J, Huang D. Regression-based algorithm for bulk motion subtraction in optical coherence tomography angiography. *Biomed Opt Express*. 2017;8:3053–3066.
6. Camino A, Zhang M, Gao SS, et al. Evaluation of artifact reduction in optical coherence tomography angiography with real-time tracking and motion correction technology. *Biomed Opt Express*. 2016;7:3905–3015.
7. Jia Y, Tan O, Tokayer J, et al. Split-spectrum amplitude-decorrelation angiography with optical coherence tomography. *Opt Express*. 2012;20:4710–4725.
8. Kraus MF, Potsaid B, Mayer MA, Bock R, Baumann B, Liu JJ, et al. Motion correction in optical coherence tomography volumes on a per A-scan basis using orthogonal scan patterns. *Biomed Opt Express*. 2012;3:1182–1199.
9. Wang RK, Jacques SL, Ma Z, Hurst S, Hanson SR, Gruber A. Three dimensional optical angiography. *Opt Express*. 2007;15:4083–4097.
10. Zhang M, Wang J, Pechauer AD, et al. Advanced image processing for optical coherence tomographic angiography of macular diseases. *Biomed Opt Express*. 2015;6:4661–4675.
11. Campbell JP, Zhang M, Hwang TS, et al. Detailed vascular anatomy of the human retina by projection-resolved optical coherence tomography angiography. *Sci Rep*. 2017;7:42201.
12. Su JP, Chandwani R, Gao SS, et al. Calibration of optical coherence tomography angiography with a microfluidic chip. *J Biomed Opt*. 2016;21:086015.
13. Yang J, Su J, Wang J, et al. Hematocrit dependence of flow signal in optical coherence tomography angiography. *Biomed Opt Express*. 2017;8:776–789.
14. Zhang Q, Lee CS, Chao J, et al. Wide-field optical coherence tomography based microangiography for retinal imaging. *Sci Rep*. 2016;6:22017.
15. Zang P, Liu G, Zhang M, et al. Automated motion correction using parallel-strip registration for wide-field en face OCT angiogram. *Biomed Opt Express*. 2016;7:2823–2836.
16. Liu G, Yang J, Wang J, et al. Extended axial imaging range, widefield swept source optical coherence tomography angiography. *J Biophotonics*. 2017;10:1464–1472.
17. Jia Y, Bailey ST, Wilson DJ, et al. Quantitative optical coherence tomography angiography of choroidal neovascularization in age-related macular degeneration. *Ophthalmology*. 2014;121:1435–1444.
18. Tang FY, Ng DS, Lam A, et al. Determinants of quantitative optical coherence tomography angiography metrics in patients with diabetes. *Sci Rep*. 2017;7:2575.
19. Gao SS, Jia Y, Liu L, et al. Compensation for reflectance variation in vessel density quantification by optical coherence tomography angiography. *Invest Ophthalmol Vis Sci*. 2016;57:4485–4492.
20. Camino A, Zhang M, Dongye C, et al. Automated registration and enhanced processing of clinical optical coherence tomography angiography. *Quant Imaging Med Surg*. 2016;6:391–401.
21. Schottenhamml J, Moult EM, Ploner S, et al. An automatic, intercapillary area based algorithm for quantifying diabetes related capillary dropout using OCT angiography. *Retina*. 2016;36(suppl 1):S93–S101.
22. Kim AY, Chu Z, Shahidzadeh A, Wang RK, Puliafito CA, Kashani AH. Quantifying microvascular density and morphology in diabetic

retinopathy using spectral-domain optical coherence tomography angiography. *Invest Ophthalmol Vis Sci*. 2016;57:OCT362–OCT370.
23. Gadde SGK, Anegondi N, Bhanushali D, et al. Quantification of vessel density in retinal optical coherence tomography angiography images using local fractal dimension. *Invest Ophthalmol Vis Sci*. 2016;57:246–252.
24. Alam M, Thapa D, Lim JI, Cao D, Yao X. Quantitative characteristics of sickle cell retinopathy in optical coherence tomography angiography. *Biomed Opt Express*. 2017;8:1741–1753.
25. Yarmohammadi A, Zangwill LM, Diniz-Filho A, et al. Optical coherence tomography angiography vessel density in healthy, glaucoma suspect, and glaucoma eyes. *Invest Ophthalmol Vis Sci*. 2016; 57:OCT451–OCT459.
26. Takusagawa HL, Liu L, Ma KN, et al. Projection-resolved optical coherence tomography angiography of macular retinal circulation in glaucoma. *Ophthalmology*. 2017;124:1589–1599.
27. Ghasemi Falavarjani K, Tsui I, Sadda SR. Ultra-wide-field imaging in diabetic retinopathy. *Vision Res*. 2017;139:187–190.
28. Hwang TS, Gao SS, Liu L, et al. Automated quantification of capillary nonperfusion using optical coherence tomography angiography in diabetic retinopathy. *JAMA Ophthalmol*. 2016; 134:367–373.
29. Zhang M, Hwang TS, Dongye C, Wilson DJ, Huang D, Jia Y. Automated quantification of nonperfusion in three retinal plexuses using projection-resolved optical coherence tomography angiography in diabetic retinopathy. *Invest Ophthalmol Vis Sci*. 2016;57:5101–5106.